

Bayesian Analysis of High-dimensional Discrete Graphical Models

Anwesha Bhattacharyya*

Department of Statistics, University of Michigan

and

Yves Atchade

Department of Statistics, Boston University

July 19, 2022

Abstract

This work introduces a Bayesian methodology for fitting large discrete graphical models with spike-and-slab priors to encode sparsity. We consider a quasi-likelihood approach that enables node-wise parallel computation resulting in reduced computational complexity. We introduce a scalable langevin MCMC algorithm for sampling from the quasi-posterior distribution which enables variable selection and estimation simultaneously. We present extensive simulation results to demonstrate scalability and accuracy of the method. We also analyze the 16 Personality Factors (PF) dataset to illustrate performance of the method.

Keywords: Discrete graphical models, networks, High-dimensional Bayesian inference, Spike-and-slab priors, Markov Chain Monte Carlo

* This work is partially supported by the NSF grant DMS 1513040. MSC 2010 subject classifications: Primary 62F15, 60K35; secondary 60K35

1 Introduction

In this paper we are primarily interested in model-based inference of networks from observed data at each node, in settings where the data can take only finite number of values. This is motivated by the widespread availability of this type of data in areas of image processing, computer science, social sciences, bio-informatics, to name a few. For example, Banerjee et al. (2008) used an Ising model to find association between voting patterns of senators from their binary voting records. Ekeberg et al. (2013) used a Potts model to predict contact between amino acids in protein chains. The Ising model Ising (1925) was originally formulated in the Physics literature as a simple model for interacting magnetic spins on a lattice. The Potts model is a generalization of the Ising model in which spins can take more than two values with more complex dependencies. These models are flexible and are used in different fields such as image analysis Besag (1986) and disease mapping Green and Richardson (2002) among others. We aim to construct robust and scalable bayesian inference procedures for these models.

Bayesian procedures have two built-in features that are in growing demand in fields such as bio-informatics (Greenfield et al. (2013); Studham et al. (2014); Peng et al. (2013)): a) the ability to incorporate existing knowledge in new data analysis, and b) a simple mechanism for uncertainty quantification. However large-scale Bayesian modeling is computationally challenging, particular when dealing with discrete graphical models. Indeed, a full Bayesian treatment of discrete graphical models lead to double-intractable posterior distributions (Murray et al. (2006)) for which specialized MCMC algorithms are needed (Zhou and Schmidler (2009); Lyne et al. (2015); Murray et al. (2006)). However these algorithms are not applicable when dealing with graphical models with very large numbers of parameters.

In the frequentist literature there is a long history of fitting discrete graphical models using (quasi/pseudo)-likelihood methods instead of the full likelihood (Besag (1974); Guyon (1995)), particularly in the high-dimensional case where the model is parametrized by a large $p \times p$ matrix (Höfling and Tibshirani (2009); Ravikumar et al. (2010); Guo et al. (2015); Roy et al. (2017)), following the seminal work of Meinshausen and Buhlmann

(2006). The approach of quasi-likelihood has also been used in bayesian settings Kato (2013), Marin et al. (2012) and references within. A common example of quasi-likelihood (popularly known as the pseudo-likelihood) is formed by taking product of the conditional distributions of each variable. It is used as a computationally efficient replacement to the true likelihood in an otherwise standard inference strategy. The form of pseudo-likelihood can be exploited to perform parallel computations. This allows us to treat the entire inferential problem as node-wise separate sub-problems reducing the computational burden significantly.

When the number of nodes (p) is large while data is limited, parameter estimation for each of the sub-problems is still difficult unless we induce sparsity and resort to variable selection. In bayesian framework the gold standard for variable selection are the spike and slab priors Mitchell and Beauchamp (1988) , George and McCulloch (1997) which are a mixture of point mass (spike) and continuous (slab) distributions. With carefully chosen slabs the resultant posteriors have good contraction rates Castillo et al. (2015), Atchade (2017). The use of quasi-Bayesian methods for large graphical models has been recently analyzed, and shown to be theoretically valid. It has been shown in Atchade (2017), that the quasi-posterior distribution for the Ising Model resulting from a degenerate spike and a Laplace slab has good contraction properties. Under certain regulatory conditions the posterior distribution on θ contracts in Frobenius norm at the rate of $O(\sqrt{\frac{(p+S)\log(p)}{n}})$, where p is the number of nodes, and S the number of edges of the true graph.

In-spite of having good theoretical properties, the drawback of a spike degenerate at 0 is that the resultant posterior distribution is not continuous on $\mathbb{R}^{p \times p}$. Such a prior is computationally difficult to handle because of the non-overlapping support of different active subsets of the parameter Atchade (2015). In high dimensions this causes a practical issue of constructing tractable sampling schemes for the resulting posterior distributions. The common approach of integrating out parameters Bottolo and Richardson (2010) fails when either the model or the prior is non-gaussian. In some cases specialized trans-dimensional MCMC with reversible jump Chen et al. (2011) are used for sampling purposes, but these do not produce chains that mix easily in higher dimensions. The natural alternative is to

relax the point mass spike and slab prior and approximate the Dirac measure at 0 through a low variance continuous distribution. Usually a Gaussian distribution is used for the spike and a more heavy tail distribution is used for the slab. Common examples of slab distributions include Gaussian distribution with high variance, Laplace distribution and Student’s t distribution.

In our paper we put together a scalable Bayesian methodology for high dimensional Potts or Ising Model using pseudo-likelihood and achieve robust estimation through the use of relaxed spike and slab prior distributions that allow sampling of the quasi-posterior distribution through standard MCMC algorithms.

The rest of the paper is organized as follows: Section 2 introduces the Potts Model, the pseudo-likelihood approach, the relaxed spike and slab prior and the resulting quasi-posterior distribution. In section 3 we propose a scalable Langevin MCMC algorithm to deal with the resulting quasi-posterior distribution. Section 4 illustrates the performance of our method through simulation results. Finally, in section 5 we present an application of our method in the context of psychological data through the analysis of the 16 Personality Factors (16PF) dataset.

2 Quasi-posterior distribution of the Potts model under spike and slab prior

An m -colored Potts model parametrized by a sparse symmetric matrix θ is a probability mass function on $\mathcal{Z} = \{0, 1, \dots, m - 1\}^p$ given by

$$f(z_1, \dots, z_p | \theta) = \frac{1}{\Psi(\theta)} \exp \left\{ \sum_{r=1}^p \theta_{rr} C(z_r) + \sum_{r=1}^p \sum_{j < r}^p \theta_{rj} C(z_r, z_j) \right\}. \quad (1)$$

Here $\Psi(\theta)$ is the normalizing constant which is obtained by summing over all possible values of the vector $z = (z_1, \dots, z_p) \in \mathcal{Z}$. The mean field function $C(\cdot)$ describes the marginal information on z_r while the coupling function $C(\cdot, \cdot)$ as suggested by the name describes

the interaction between z_r and z_j . A special case of (1) is the Ising Model where m is 2, hence $\mathcal{Z} = \{0, 1\}^p$. In case of the Ising model the mean field and the coupling functions are typically taken as identity ($C(z_r) = z_r$) and multiplicative ($C(z_r, z_j) = z_r z_j$) respectively.

The problem of interest in this work is the estimation and recovery of the sparse matrix θ based on sample observations $\{z^i\}_{i=1}^n$, where $z^i = (z_1^i, \dots, z_p^i) \in \mathcal{Z}$ is the i th observation. We use $Z \in \{0, \dots, m-1\}^{n \times p}$ to denote the matrix of observations, where the i -th row of Z is z^i . The likelihood of θ can then be expressed as

$$\mathcal{L}^n(\theta|Z) = \prod_{i=1}^n f(z^i|\theta) = \prod_{i=1}^n \frac{1}{\Psi(\theta)} \exp \left\{ \sum_{r=1}^p \theta_{rr} C(z_r^i) + \sum_{r=1}^p \sum_{j<r}^p \theta_{rj} C(z_r^i, z_j^i) \right\}.$$

In a high-dimensional setting (typically $p > n$, $\frac{\log(p)}{n} \rightarrow 0$), likelihood based inference on θ is computationally intractable because of the normalization constant $\Psi(\theta)$. Note that, the number of summands in $\Psi(\theta)$ is exponential in p , and quickly blows up for even moderate values of p .

2.1 Quasi(Pseudo)-likelihood

Following an approach widely adopted in the high-dimensional frequentist literature, we explore the use of quasi(pseudo)-likelihoods in the Bayesian treatment of discrete graphical models. The conditional distribution for the r th node (given all other nodes) in a Potts model for the i th observation z^i can be written as

$$f(z_r^i | z_{\setminus r}^i, \theta_r) = \frac{1}{\Psi_r^i(\theta_r)} \exp \left\{ \theta_{rr} C(z_r^i) + \sum_{j \neq r} \theta_{rj} C(z_r^i, z_j^i) \right\}. \quad (2)$$

where $z_{\setminus r}^i = (z_1^i, \dots, z_{r-1}^i, z_{r+1}^i, \dots, z_p^i)'$ and $\theta_r = (\theta_{r1}, \dots, \theta_{rp})'$ is the r th column of θ . The normalizing constant of this conditional distribution is given by

$$\Psi_r^i(\theta_r) = \sum_{s=0}^{m-1} \exp \left(\theta_{rr} C(s) + \sum_{j \neq r} \theta_{rj} C(s, z_j^i) \right).$$

Computing $\Psi_r^i(\theta_r)$ requires $O(p \times m)$ units of operations and hence is scalable when m is small.

We denote the r_{th} conditional log-likelihood as $\ell_r^n(\theta|Z)$ and express the log pseudo-likelihood as

$$\begin{aligned} \ell^n(\theta|Z) &= \sum_{r=1}^p \ell_r^n(\theta_r|Z) \\ &= \sum_{r=1}^p \sum_{i=1}^n \left[\theta_{rr} C(z_r^i) + \sum_{j \neq r} \theta_{rj} C(z_r^i, z_j^i) \right. \\ &\quad \left. - \log \left(\sum_{s=0}^{m-1} \exp \left(\theta_{rr} C(s) + \sum_{j \neq r} \theta_{rj} C(s, z_j^i) \right) \right) \right]. \end{aligned} \quad (3)$$

Note that the ability to write the log pseudo-likelihood $\ell^n(\theta|Z)$ as sum of log conditional likelihoods $\ell_r^n(\theta_r|Z)$ allows us to transform the inference on $\theta \in \mathbb{R}^{p \times p}$ into p separable sub-problems on \mathbb{R}^p . However the symmetry of the matrix θ is lost, and we get two estimates for each component θ_{ij} . Following Meinshausen and Bühlmann (2006) we resolve this issue at the post-inference stage by taking an aggregate of the two estimates. In the data analysis section we discuss possible methods for aggregating the estimates.

2.2 Spike and slab prior

To take advantage of the factorized form of the pseudo-likelihood function from (3) we will assume in our prior distribution that the columns of θ are independent. We note that it is a common practice in Bayesian data analysis to ignore unknown dependence structure among parameters in the prior distribution when dealing with multivariate parameters. These dependences are then learned from the data in the posterior distribution. The lack of symmetry is more problematic, and are dealt with at the post-inference stage.

As a prior distribution for θ_r we propose to use a relaxed form of the spike and slab prior (Mitchell and Beauchamp (1988); George and McCulloch (1997)). More specifically, for each parameter $\theta_r \in \mathbb{R}^p$, $r = 1, \dots, p$, we introduce a selection parameter $\delta_r = (\delta_{r1}, \dots, \delta_{rp}) \in \Delta$, where $\Delta = \{0, 1\}^p$. We assume that the component of δ_r have independent Bernoulli prior distributions, so that the joint distribution of δ_r writes

$$\omega_{\delta_r} = \prod_{j=1}^p q^{\delta_{rj}} (1-q)^{1-\delta_{rj}} ; q = p^{-(u+1)} ; u > 0 \quad (4)$$

where u is a hyper-parameter. The conditional distribution of θ_r given δ_r is given by

$$\begin{aligned}\theta_{rj}|\{\delta_{rj} = 1\} &\sim \mathbf{Laplace}(\rho_r); \rho_r > 0 \\ \theta_{rj}|\{\delta_{rj} = 0\} &\sim \mathbf{N}(0, \gamma); \gamma > 0,\end{aligned}\tag{5}$$

for hyper-parameters $\gamma > 0$ and $\rho_r > 0$. The Gaussian distribution $\mathbf{N}(0, \gamma)$ is used to approximate the Dirac point mass at 0 commonly used in strict spike and slab prior. Hence γ is chosen as a small constant. We further discuss the choice of γ and u below. Since ρ_r is more difficult to choose and our inference is sensitive to such choice, we shall treat ρ_r as a parameter with an improper prior $\pi(\rho_r) \propto \mathbf{1}_{(0, \infty)}(\delta_r)$.

We introduce the notations $\theta_{r\delta_r} = (\theta_{rj} \text{ s.t. } \delta_{rj} = 1) \in \mathbb{R}^{\|\delta_r\|_1}$, $\delta_r^c = 1 - \delta_r$, $\|z\|_1 = \sum_{j=1}^p |z_j|$ and $\|z\|_2 = \sqrt{\sum_{j=1}^p z_j^2}$. Using this notation, and writing $\delta = (\delta_1, \dots, \delta_p)$, $\theta = (\theta_1, \dots, \theta_p)$ and $\rho = (\rho_1, \rho_2, \dots, \rho_p) \in \mathbb{R}^p$, the joint prior distribution of $(\delta, \theta, \rho) \in \Delta^p \times \mathbb{R}^{p \times p} \times \mathbb{R}_+^p$ is given by

$$\pi(\delta, d\theta, d\rho) = \prod_{r=1}^p \pi(\delta_r, d\theta_r, d\rho_r),$$

where the prior distribution of $(\delta_r, \theta_r, \rho_r)$ on $\Delta \times \mathbb{R}^p \times (0, \infty)$ can be written as

$$\pi(\delta_r, d\theta_r, d\rho_r) \propto \omega_{\delta_r} \left(\frac{\rho_r}{2}\right)^{\|\delta_r\|_1} (2\pi\gamma)^{\frac{\|\delta_r\|_1}{2}} \exp\left(-\rho_r \sum_{j: \delta_{rj}=1} |\theta_{rj}| - \frac{1}{2\gamma} \sum_{j: \delta_{rj}=0} \theta_{rj}^2\right) d\theta_r d\rho_r.\tag{6}$$

2.3 Quasi-posterior distribution

By combining the conditional-likelihood function for the r_{th} column θ_r of θ , and the prior distribution given in (6), we obtain a quasi-posterior distribution on $\Delta \times \mathbb{R}^p \times \mathbb{R}_+^p$ given by

$$\begin{aligned}\Pi_n(\delta_r, d\theta_r, d\rho_r|Z) \\ \propto \omega_{\delta_r} \left(\frac{\rho_r \sqrt{\pi\gamma}}{\sqrt{2}}\right)^{\|\delta_r\|_1} \exp\left(\ell_r^n(\theta_r|Z) - \rho_r \sum_{j: \delta_{rj}=1} |\theta_{rj}| - \frac{1}{2\gamma} \sum_{j: \delta_{rj}=0} \theta_{rj}^2\right) d\theta_r d\rho_r.\end{aligned}\tag{7}$$

We multiplicatively combine these p quasi-posterior distributions to obtain the full quasi-posterior distribution on (δ, θ, ρ) given by

$$\Pi_n(\delta, d\theta, d\rho|Z) = \prod_{r=1}^p \Pi_n(\delta_r, d\theta_r, d\rho_r|Z). \quad (8)$$

The choice of prior that we have proposed in (6), leads to a quasi-posterior distribution that is easy to handle with standard MCMC algorithms and behaves well under suitable choice of hyper-parameters.

2.4 Choice of hyper-parameters

The selection hyper-parameter q in (4) is set at $q = \frac{1}{p^{1+u}}$, for some constant $u > 0$. This choice of q is known to yield good posterior contraction properties (see e.g. Atchade (2017)).

The hyper-parameter γ in (6) is associated with the inactive components. A high value of γ typically results in a faster convergence of the MCMC sampler (Section 3), but it also distorts the shape of the quasi-posterior (8) leading to larger statistical errors. Thus the choice of γ requires careful consideration. Choosing γ to be a constant of the order of $O(np)^{-1}$ worked well in our simulation settings as well as data analysis.

2.5 Post estimation symmetrization

A consequence of parallel computation is the breakdown of the inherent symmetry of the parameter of interest θ . Parallel computation at node i and node j results in two different set of estimates $\hat{\theta}_{ij}$ and $\hat{\theta}_{ji}$ for the same parameter. For the sake of interpretation it is useful to provide a single estimate and credible interval corresponding to the parameter θ_{ij} evaluating the strength of connection between node i and j . We propose a post-estimation symmetrization resulting in a singular estimate

$$\tilde{\theta}_{ij} = \frac{\hat{\theta}_{ij} + \hat{\theta}_{ji}}{2}. \quad (9)$$

The credible region corresponding to the parameter θ_{ij} can be constructed using a union of the 95% credible intervals estimated from the quasi-posterior distribution of θ_{ij} and

θ_{ji} . Taking the union of the credible intervals is a conservative approach as opposed to taking the intersection. However it always provides a concrete interval or set unlike the intersection in which case the credible intervals may be too short or in some cases even result in null set. We can evaluate the discrepancy in the two sets of estimates through a measure of concordance given as

$$\text{Measure of concordance for edge } i\text{-}j = \frac{\text{length}(c_{ij} \cap c_{ji})}{\text{length}(c_{ij} \cup c_{ji})}. \quad (10)$$

Here c_{ij} (resp. c_{ji}) are the credible intervals for θ_{ij} (resp. θ_{ji}).

Note that δ_{ij} are auxiliary parameters and not of immediate interest. However they can be used to estimate the probability of an edge between node (i, j) . A conservative estimate of this probability can be obtained as

$$\hat{p}_{ij} = P(\text{edge between node } i \text{ and } j) = \min(\hat{P}(\delta_{ij} = 1), \hat{P}(\delta_{ji} = 1)). \quad (11)$$

3 MCMC Sampling Algorithm

In this section we shall discuss in details the construction of a Markov Chain Monte Carlo (MCMC) algorithm to draw Monte Carlo samples from the posterior distribution (8). By virtue of independence, it is enough to draw sample for each of the joint variable $(\theta_r, \delta_r, \rho_r)$. Large efficiency gain is possible by performing these simulations in parallel.

We use a Metropolis-Hastings within Gibb Sampler, where we update the active components $\theta_{r\delta_r}$ given $(\delta_r, \theta_{r\delta_r^c}, \rho_r)$, then update the inactive components $\theta_{r\delta_r^c}$ given $(\delta_r, \theta_{r\delta_r}, \rho_r)$, then update δ_r given (θ_r, ρ_r) , and finally update ρ_r given (δ_r, θ_r) . Here we have used the notations $\theta_r = [\theta_{r\delta_r}, \theta_{r\delta_r^c}]$, where $\theta_{r\delta_r}$ regroups the components of θ_r for which $\delta_{rj} = 1$, and $\theta_{r\delta_r^c}$ regroups the remaining components. We refer the reader to Robert and Casella (2004) for an introduction to basic MCMC algorithms.

3.1 Metropolis Adjusted Langevin Algorithm (MALA) for active parameters

Suppose that δ_r is such that $0 < \|\delta_r\|_1 < p$. We update $\theta_{r\delta_r}$ by a Metropolis Adjusted Langevin Algorithm. Other algorithms including Hamiltonian Monte Carlo can be used as well. We refer the reader to Liu (2001); Robert and Casella (2004)) for more details on MCMC. We define

$$h_\gamma(\delta_r, \theta_r, \rho_r; z) = \left[\ell_r^n(\theta_r|z) - \rho_r \|\theta_{r\delta_r}\|_1 - \frac{1}{2\gamma} \|\theta_{r\delta_r}\|_2^2 \right]. \quad (12)$$

The function $\theta_r \rightarrow h_\gamma(\delta_r, \theta_r, \rho_r; z)$ has a sub-gradient given by

$$\nabla_{\theta_r} h_\gamma(\delta_r, \theta_r, \rho_r; z) = \nabla_{\theta_r} \ell_r^n(\theta_r|z) - \rho_r \times \text{sgn}(\theta_{r\delta_r}) - \frac{1}{\gamma} \theta_{r\delta_r}.$$

We further define the truncated gradient (Atchade (2006))

$$G_\gamma(\delta_r, \theta_r, \rho_r; z) \stackrel{\text{def}}{=} \frac{c}{c \vee \|\nabla_{\theta_r} h_\gamma(\delta_r, \theta_r, \rho_r; z)\|_2} \nabla_{\theta_r} h_\gamma(\delta_r, \theta_r, \rho_r; z), \quad (13)$$

for some positive constant c , where $a \vee b = \max(a, b)$. We update (one at the time) the selected components of θ_r as follows. Given j such that $\delta_{rj} = 1$, we propose

$$\theta_{rj}^{prop} | \theta_r \sim N\left(\theta_{rj} + \frac{\sigma}{2} [G_\gamma(\delta_r, \theta_r, \rho_r; z)]_j, \sigma^2\right), \quad (14)$$

where σ is some constant step size and $[G_\gamma(\delta_r, \theta_r, \rho_r; z)]_j$ represents the j th component of $G_\gamma(\delta_r, \theta_r, \rho_r; z)$. Let $g(\theta_{rj}^{prop} | \theta_r)$ denote the density of the above proposal distribution in (14). We also define $\theta_r^{prop} = [\theta_{r1}, \dots, \theta_{rj-1}, \theta_{rj}^{prop}, \theta_{rj+1}, \dots, \theta_{rp}]$ and the acceptance probability as

$$\text{Acc}_{rj} = \min\left(1, \frac{g(\theta_{rj} | \theta_r^{prop})}{g(\theta_{rj}^{prop} | \theta_r)} \times \frac{\Pi_n(\delta_r, \theta_r^{prop}, \rho_r | Z)}{\Pi_n(\delta_r, \theta_r, \rho_r | Z)}\right). \quad (15)$$

With probability Acc_{rj} we set $\theta_{rj} = \theta_{rj}^{prop}$, and with probability $1 - \text{Acc}_{rj}$, we do nothing. In other word, we update the component θ_{rj} according to the Truncated Metropolis Adjusted Langevin Algorithm (MALA) (Atchade (2006)). In our simulations the step size σ is kept constant. Alternatively, it can also be updated for each θ_{rj} in the spirit of an adaptive MCMC scheme if so desired.

Finally we note that, under sparse prior the number of active parameters in each node is small. So we may choose to update the active parameters at a node one by one without losing computational efficiency.

3.2 Independent sampler for updating inactive parameters

Under sparsity, the number of inactive components of θ_r is large and hence updating them one by one, using Langevin MCMC is computationally expensive. Instead we update the inactive $\theta_{r\delta_r^c}$ given $(\delta_r, \theta_{r\delta_r})$ using an independent Metropolis sampler. Let

$$H_r \stackrel{\text{def}}{=} \nabla^{(2)} \ell_r^n([\theta_{r\delta_r}, 0]|z) = \begin{bmatrix} [H_r]_{\delta_r} & [H_r]_{\delta_r, \delta_r^c} \\ [H_r]_{\delta_r, \delta_r^c} & [H_r]_{\delta_r^c} \end{bmatrix}. \quad (16)$$

Let k_γ be an approximation of h_γ in (12) where $\ell_r^n(\theta_r|z)$ is substituted by its second-order Taylor's expansion around $[\theta_{r\delta_r}, 0]$. Hence,

$$k_\gamma(\delta_r, [\theta_{r\delta_r}, \theta_{r\delta_r^c}]; z) = \frac{1}{2}(\theta_{r\delta_r^c} - \mu)' \Sigma^{-1}(\theta_{r\delta_r^c} - \mu) + \text{const.}$$

Here $\Sigma = \gamma(I_{\delta_r^c} - \gamma[H_r]_{\delta_r^c})^{-1}$, $\mu = \Sigma([\nabla \ell_r([\theta_{r\delta_r}, 0]|z)]_{\delta_r^c})$ and the constant term is a function of $\theta_{r\delta_r}$, independent of $\theta_{r\delta_r^c}$. Note that $[\nabla \ell_r([\theta_{r\delta_r}, 0]|z)]_{\delta_r^c}$ is the sub-vector of the first derivative indexed by the components δ_r^c . Hence for fixed ρ_r, δ_r and $\theta_{r\delta_r}$ we sample $\theta_{r\delta_r^c}$ using an independent Metropolis sampler with proposal $N(\mu, \Sigma)$.

While this proposal distribution has a high acceptance probability, it involves the computation of the inverse of a large matrix $[H_r]_{\delta_r^c}$ which adds to the computational burden. We propose two modifications to the computations, (1) reduces burden in terms of sample size n and (2) reduces burden in terms of number of nodes p . These modifications are made to the proposal distribution and as long as we use appropriate acceptance probability to make the Metropolis update, we are still sampling from the original quasi-posterior distribution given in (8). For the first modification, we express the double derivative as

$$-\nabla^{(2)} \ell_r^n([\theta_r]|z) = [C_r - \mathbf{E}[C_r]]' W(\theta_r) [C_r - \mathbf{E}[C_r]]$$

where $W(\theta_r)$ is a diagonal matrix of order $mn \times mn$ and $(C_r$ and $\mathbf{E}[C_r])$ are matrices of order $mn \times p$ where m denotes the number of discrete values each node can take.

(Details are in Appendix A 7). The computation of the double derivative thus roughly takes $O(n^2m^2p)$ operations when m is small. The computational burden grows with n and we try to control it by taking an approximation of the double derivative using weighted sampling. We draw a without replacement weighted subsample of size η from the diagonal terms of $W(\theta_r)$ where the weights $\{\omega_k\}_{k=1}^{mn}$ are taken to be $\omega_k \propto \| [C_r - \mathbf{E}[C_r]]_k \|_2 \times W(\theta_r)_k$. Here $[C_r - \mathbf{E}[C_r]]_k$ is the k th row of the matrix $[C_r - \mathbf{E}[C_r]]$. We take an approximation of $-\nabla^{(2)}\ell_r^n(\theta_r|z)$ by multiplying only the sub-matrices obtained through this sampling scheme. The approximation is hence defined as

$$-\nabla^{(2)}\ell_{r,approx}^n(\theta_r|z) = [C_r - \mathbf{E}(C_r)]'_{p \times \eta} W(\theta_r)_{\eta \times \eta} [C_r - \mathbf{E}(C_r)]_{\eta \times p}, \quad (17)$$

$$\hat{H}_r = \nabla^{(2)}\ell_{r,approx}^n([\theta_{r\delta_r}, 0]|z). \quad (18)$$

The size of weighted subsample η , can take any value between $(0, m \times n)$. The choice of η involves a trade-off between accuracy of approximation and the computational burden. Higher value of η yields closer approximation to the double derivative while a lower value of η affords faster computation. The algorithm implemented in MATLAB (Supplementary) uses the parameter **sam** to denote η . Thus the first modification substitutes H_r by \hat{H}_r

The computation of Σ involves inversion of a matrix of order nearly $p \times p$ which is computationally expensive for large p . To avoid this, we propose the second modification of the independent sampler. We once again use a Metropolis within Gibbs strategy to implement a block-by-block update of the inactive parameters. We can partition the inactive parameters for the r th node as $\theta_{r\delta_r^c} = [u_1, u_2, \dots, u_b]$. Instead of updating $\theta_{r\delta_r^c}$ as a whole, we update each block $u_j; j = 1, \dots, b$. We use the notation $u_{\setminus k}$ to denote $[u_1, \dots, u_{k-1}, u_{k+1}, \dots, u_b]$ and express $\theta_{r\delta_r^c} = [u_k, u_{\setminus k}]$ by regrouping the elements. We exploit the same idea of substituting $\ell_r^n([\theta_{r\delta_r}, \theta_{r\delta_r^c}]|z)$ by its Taylor's expansion around $[\theta_{r\delta_r}, 0, u_{\setminus k}]$ as in 12. Thus we perform the update of the inactive parameters in b steps updating b blocks one-by one.

The final proposal distribution for updating u_k is given as $N(\mu_k, \Sigma_k)$ where

$$u_k^{prop} | \theta_r \sim N(\mu, \Sigma); \quad (19)$$

$$\mu_k = \Sigma_k([\nabla \ell_r^n([\theta_{r\delta_r}, 0, u_{\setminus k}]|z)]_{\delta_{u_k}}), \quad (20)$$

$$\Sigma_k = \gamma(I_{\delta_{u_k}} - \gamma[\hat{H}_r]_{\delta_{u_k}})^{-1}. \quad (21)$$

Here $[\nabla \ell_r^n([\theta_{r\delta_r}, 0, u_{\setminus k}]|z)]_{\delta_{u_k}}$ is the sub-vector of $\nabla \ell_r^n([\theta_{r\delta_r}, 0, u_{\setminus k}]|z)$ corresponding to the elements of u_k and similarly $[\hat{H}_r]_{\delta_{u_k}}$ is the sub-matrix of \hat{H}_r corresponding to the elements of u_k . Note that the argument of \hat{H}_r should ideally change for each block according to the Taylor's approximation but we choose to use the same \hat{H}_r as in (18) to avoid multiple computations of large order. Let $g(u_k^{prop} | \theta_r)$ denote the density of the proposal distribution in (19)-(21) and $\theta_r^{prop} = [\theta_{r\delta_r}, u_k^{prop}, u_{\setminus k}]$.

We define the acceptance probability as

$$\text{Acc}(u_k, u_k^{prop}) = \min \left(1, \frac{g(u_k | \theta_r^{prop})}{g(u_k^{prop} | \theta_r)} \times \frac{\Pi_n(\delta_r, \theta_r^{prop}, \rho_r | Z)}{\Pi_n(\delta_r, \theta_r, \rho_r | Z)} \right) \quad (22)$$

and use this to update the block u_k using a Metropolis Hastings step. (A few other implementation details regarding the block updates is discussed in Appendix B [7])

3.3 Independent Bernoulli sampler for selection parameters

Equation (7) is used to show that given $(\theta_r ; \rho_r, \gamma, u)$ the δ_{rj} 's are conditionally independent.

In fact

$$\delta_{rj} | \theta_r \sim \text{Ber}(p_{rj}) ; p_{rj} = \frac{\frac{q}{1-q} \frac{\rho_r}{2} \sqrt{2\pi\gamma} e^{\tau_{rj}(\delta_r, \theta_r, \rho_r)}}{1 + \frac{q}{1-q} \frac{\rho_r}{2} \sqrt{2\pi\gamma} e^{\tau_{rj}(\delta_r, \theta_r, \rho_r)}}, \quad (23)$$

where

$$\tau_{rj}(\delta_r, \theta_r, \rho_r) \stackrel{\text{def}}{=} \frac{1}{2\gamma} \theta_{rj}^2 - \rho_r |\theta_{rj}| \text{ for } j = 1, \dots, p.$$

This ensures highly efficient sampling of the selection parameters δ_r 's.

3.4 Updating ρ_r by Random Walk Metropolis

We update ρ_r using an adaptive random walk Metropolis-Hastings step based on Gaussian proposal distribution given as

$$\rho_r^{prop} \sim N(\rho_r, \exp(\tau)). \quad (24)$$

Keeping in mind that $\rho_r > 0$, we reject ρ_r^{prop} if $\rho_r^{prop} \leq 0$. Else, we compute the acceptance probability as

$$\text{Acc}(\rho_r, \rho_r^{prop}) = \min \left(1, \frac{g(\rho_r | \rho_r^{prop})}{g(\rho_r^{prop} | \rho_r)} \times \frac{\Pi_n(\delta_r, \theta_r, \rho_r^{prop} | Z)}{\Pi_n(\delta_r, \theta_r, \rho_r | Z)} \right) \quad (25)$$

where $g(\rho_r^{prop} | \rho_r)$ is the density of the proposal distribution (24). We update ρ_r in a Metropolis Hastings step using the acceptance probability (25). For improved mixing, we adaptively tune the scale parameter (τ) using the adaptive MCMC with varying compact sets as in Atchade and Fort (2012).

The overall MCMC sampler can be summarized as follows.

Algorithm 1. For each node $r \in \{1, \dots, p\}$ do the following.

1. Initialize with $(\theta_r^{(0)}, \delta_r^{(0)})$
2. At the t -th iteration, given $\delta_r^{(t-1)} = \check{\delta}$ and $\theta_r^{(t-1)} = \check{\theta}$, do
 - (a) For each j such that $\check{\delta}_j = 1$, we update $\check{\theta}_j$ using the MALA algorithm described in (14) and (15).
 - (b) We partition $\check{\theta}_{\delta_c}$ into b blocks $[u_1, u_2, \dots, u_b]$ that we update one by one using the Independent Metropolis with proposal (19)-(21) and acceptance probability given in (22).
 - (c) Set $\theta_r^{(t)} = \check{\theta}$. For each j in $\{1, \dots, p\}$, we update $\check{\delta}_j \sim \text{Ber}(p_j | \check{\theta})$ where the Bernoulli probability p_j is as defined in (23). Set $\delta_r^{(t)} = \check{\delta}$.
 - (d) Given $\delta_r^{(t)} = \check{\delta}$ and $\theta_r^{(t)} = \check{\theta}$, update $\rho_r^{(t)}$ by Random Walk Metropolis using (24)-(25) as described in Subsection 3.4 .

4 Simulation studies

In the simulation studies, we focus only on the Ising Model which is a special case of the Potts Model as discussed in section 2. The Ising model is used for modeling networks with nodes taking binary values only. We present the results based on two networks, one where the structure is completely random (Figure 1) and the other where it consists of clusters along the diagonals (Figure 2).

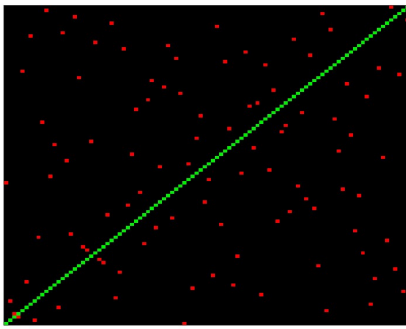


Figure 1: Heatmap of θ_* for network 1

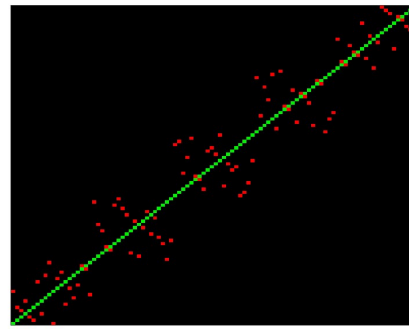


Figure 2: Heatmap of θ_* for network 2

The red and green dots indicate positive and negative values of θ_{ij} respectively

We introduce the norm $\|\theta\|_0$ as a measure of sparsity where

$$\|\theta\|_0 = \sum_{r=1}^p \sum_{j=1}^p \mathbb{1}[\theta_{rj} \neq 0].$$

For each of the two networks, the generating matrix θ_* is symmetric in $\mathbb{R}^{100 \times 100}$. Both the networks have 100 non-zero values along the diagonal of θ_* and 50 active edges out of 4950 edges, resulting in $\|\theta_*\|_0 = 200$.

Ising model is widely known for its usage in identification of phase transition properties Georgii (1988). The phase transition properties of the Ising model may lead to nodes on graph with low or completely no variability for certain choices of parameter θ_* Li and Zhang (2010). We carefully chose θ_{*ij} to avoid these scenarios. The diagonals of generating matrix

θ_* were chosen to be -2 and the non-zero off-diagonal θ_{*ij} 's to be 4 . We generate the data from the Ising model using a Gibbs sampler.

The initialization of the MCMC values can be done randomly but the mixing will be much slower in this case. We choose to use the frequentist estimate as initial value at each node r obtained through a proximal gradient descent on the corresponding conditional likelihood Parikh and Boyd (2013).

To measure convergence of the MCMC we use the relative error and the F1 score defined as,

$$\text{relative error of node } r \text{ at iteration } t = e_r^{(t)} \stackrel{\text{def}}{=} \frac{\|\theta_r^{(t)} - \theta_{*r}\|_2}{\|\theta_{*r}\|_2},$$

$$\text{relative error at iteration } t \text{ averaged across nodes} = e^{(t)} \stackrel{\text{def}}{=} \frac{\sum_{r=1}^p e_r^{(t)}}{p},$$

$$\text{F1 score of node } r \text{ at iteration } t = \text{F1}_r^{(t)} \stackrel{\text{def}}{=} \frac{2 * TA_r^{(t)} * PA_r^{(t)}}{TA_r^{(t)} + PA_r^{(t)}},$$

and

$$\text{F1 score at iteration } t \text{ averaged across nodes} = \text{F1}^{(t)} \stackrel{\text{def}}{=} \frac{\sum_{r=1}^p \text{F1}_r^{(t)}}{p}.$$

We further define,

$TA_r^{(t)}$ = proportion of true active out of predicted active θ_{rj} in node r at iteration t and

$PA_r^{(t)}$ = proportion of predicted active out of true active θ_{rj} in node r at iteration t

F1 score is the combined measure of the power of a method and it's control over false discoveries. A high F1 score indicates low type 1 error and high power.

4.1 Comparison of sample size

We generated 1,000 observations and studied the effect of sample size on the convergence of the MCMC. We ran the MCMC for 30,000 iterations. Figures 3 and 4 show the behavior of the MCMC in the first 6,000 iterations. Since we started with good initialization based on

the frequentist estimate, the MCMC has reached stable behavior within the first 100 iterations. We can see a substantial increase in performance when the sample size grows from 200 to 500. At 500 sample size the method already achieves a perfect F1 score and there is not much gain in terms of precision of estimate as sample size is increased further to 1,000. The sampler appears to perform equally well for the two networks. The relative errors and F1 scores averaged both over the nodes and the last 5,000 iterations are presented in Table 1.

		Average Relative Error	Average F1 score
Network 1 p = 100	n = 1,000	0.1128	1.0000
	n = 500	0.1320	1.0000
	n = 200	0.2697	0.9189
Network 2 p = 100	n = 1,000	0.1126	1.0000
	n = 500	0.1248	1.0000
	n = 200	0.2213	0.9533

Table 1: Table showing average relative errors and average F1 scores (recovery) for the two networks and different sample sizes. The measures were averaged over both the 100 nodes as well as the last 5,000 iterations after a burn-in of 25,000 iterations.

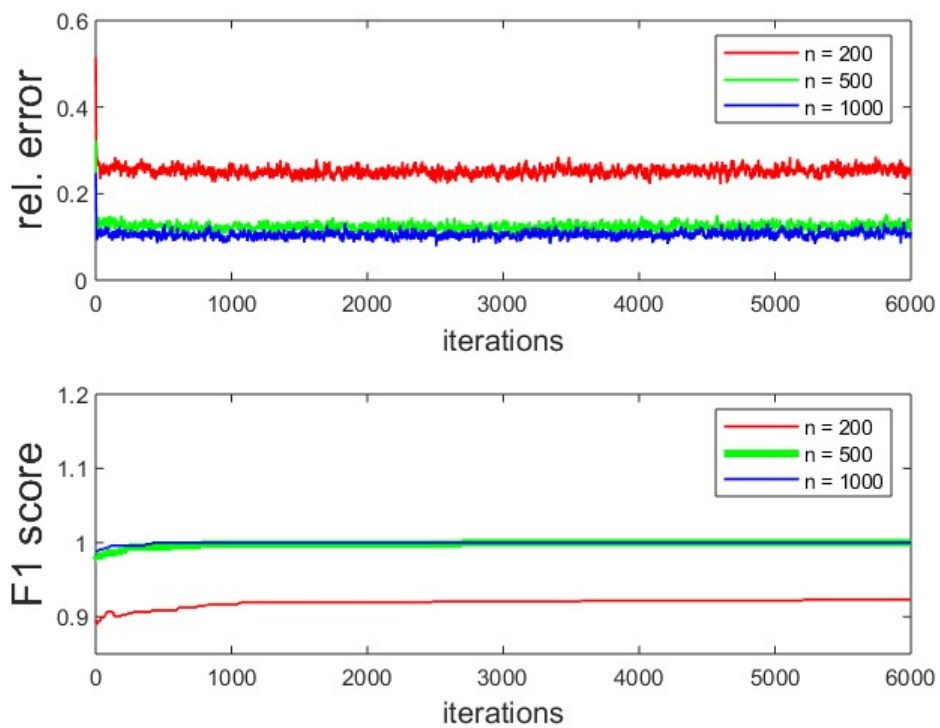


Figure 3: MCMC convergence for network 1

Top panel shows the relative error averaged across 100 nodes for the first 6,000 iterations. Bottom panel shows the F1 score (recovery) averaged across 100 nodes for the first 6,000 iterations. Sample sizes are 200 (red), 500 (green) and 1,000 (blue)

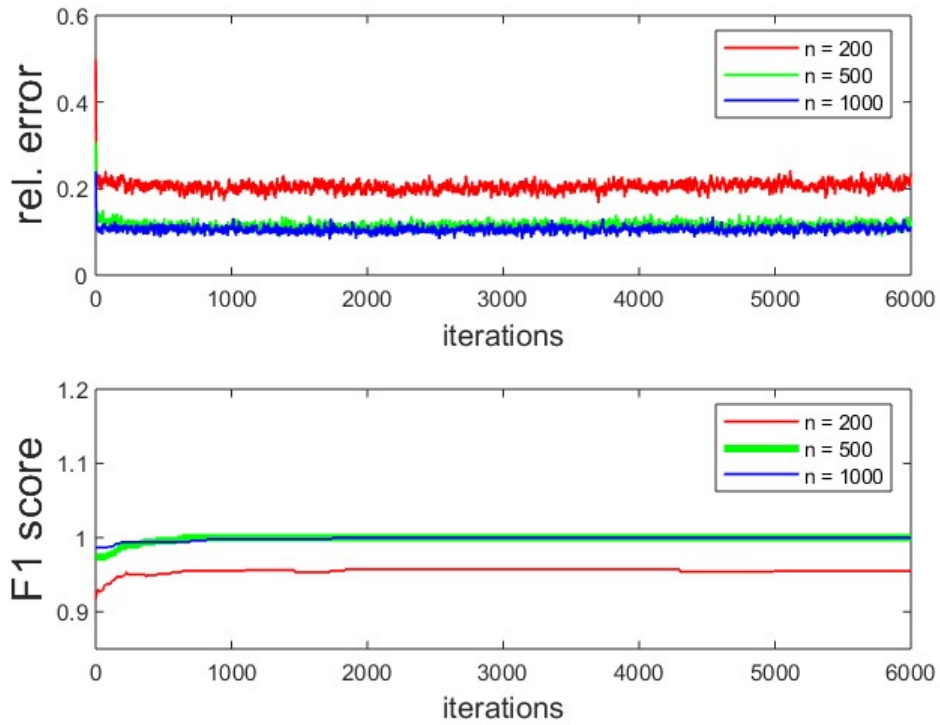


Figure 4: MCMC convergence for network 2

Top panel shows the relative error averaged across 100 nodes for the first 6,000 iterations. Bottom panel shows the F1 score (recovery) averaged across 100 nodes for the first 6,000 iterations. Sample sizes are 200 (red), 500 (green) and 1,000 (blue)

4.2 Study of credible intervals for network with 300 nodes

We generate a larger network with 300 nodes and 2,000 observations. Here θ_* is symmetric in $\mathbb{R}^{300 \times 300}$ with $\|\theta_*\|_0 = 660$. The non-zero off-diagonal values of θ_* are set at 4 and the diagonals of θ_* are either -2 or -4 . The settings were changed slightly again keeping in mind the phase transition properties of the Ising Model. In this setup, we specifically look at the credible intervals estimated through the MCMC samples. After a burn-in of 10,000 iterations, the estimates of each θ_{ij} are obtained by taking the mean of 500 samples, keeping the sample from every 100th iteration. The relative error for these 500 samples averaged across the 300 nodes is **0.1136** while the recovery(F1 score) is estimated to be **1.0000**. We obtain the final estimate of $\tilde{\theta}$ after symmetrization of the estimates as mentioned in (9). For the credible interval of θ_{*ij} we use the union of the 95% credible intervals of θ_{ij} and that of θ_{ji} . Our simulations show that the inference for θ_{ij} and θ_{ji} are consistent with measure of concordance (10) at each pair of nodes mostly above 95%. Figures 5 and 6 show the credible intervals of the active and inactive θ_{ij} separately. We also include the estimates and the true value of the parameter to show the accuracy of the estimates. A large proportion (47% approximately) of the inactive parameters are estimated to be exactly 0. The average credible intervals for each of the 4 distinct true parameter values are given in table 2 .

True parameter value	Average Credible Interval
0	$(19525 \times 10^{-8}, 19534 \times 10^{-8})$
-4	$(-5.45, -3.04)$
-2	$(-2.67, -1.41)$
4	$(2.90, 5.45)$

Table 2: Table showing Credible Intervals average for each of the four unique parameter values in the matrix θ_*

The total computing time of our method for this network with 300 nodes and 2000 observations was approximately 300 CPU-hours. We parallelized the MCMC into 40 parallel processes and the simulation was completed in approximately 7 hours. Given this, we can

say that our method is computationally scalable in these data dimensions.

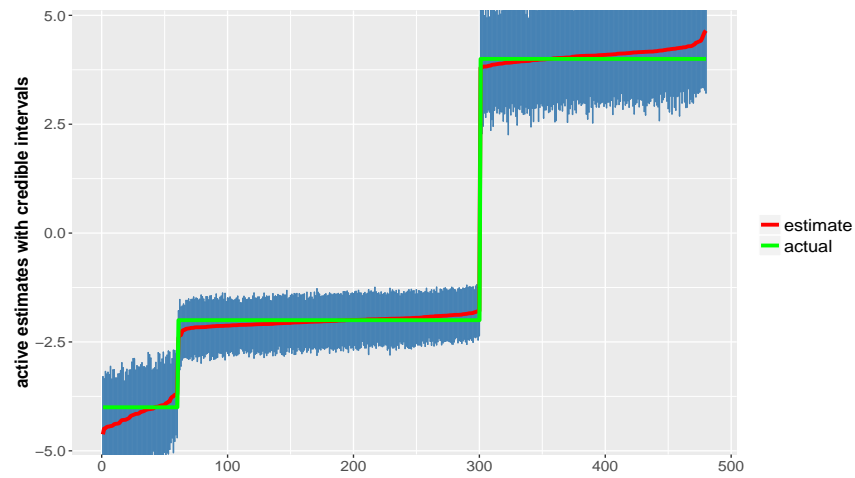


Figure 5: Credible intervals of active θ_{ij} in order of strength of estimates

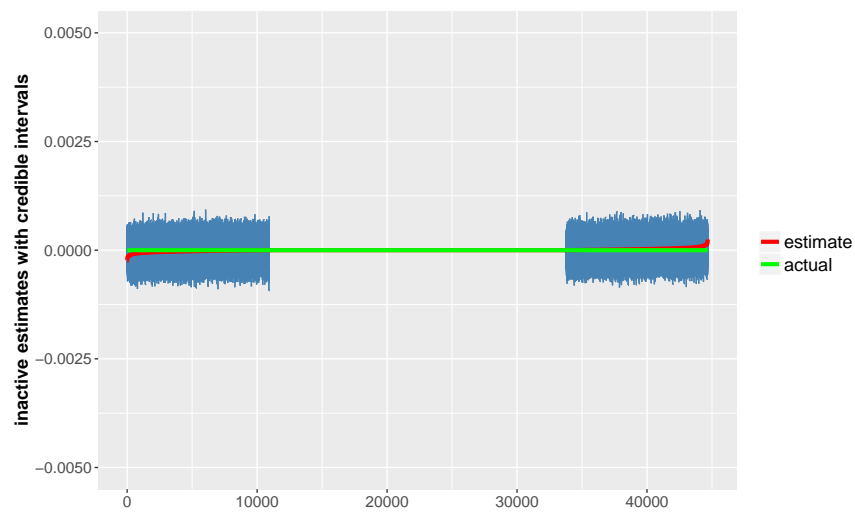


Figure 6: Credible intervals of inactive θ_{ij} in order of strength of estimates

5 Real data analysis

According to British psychologist Raymond Cattell, variations in human personality could be best explained by a model containing sixteen variables (personality factors/traits) Cattell and Mead (2008) The data that we have analyzed (source: https://openpsychometrics.org/_rawdata/), comes from an interactive questionnaire of 163 questions designed to measure Cattell’s 16 Personality Factors (16PF). For each question, a self-assigned score indicates how accurate it is on a scale of (1) disagree (2) slightly disagree (3) neither agree nor disagree (4) slightly agree (5) agree. Additionally, some other information is collected which includes the test taker’s home country, the source from which (s)he got information about the test, her/his perceived accuracy about the answers (s)he provided, age, gender and time elapsed to complete the test. In our analysis, we focused on women in the age group of 30 to 50, who had a self-reported accuracy $\geq 75\%$ and finished the test within half an hour.

The selected data had 4,162 individuals answering 163 questions. Some of the observations had missing values which are represented as 0. The proportion of missing values varied from 0.4% to 1% across different questions. The missing values were treated as missing at random and each of them were substituted by a value between 1 to 5. This value was sampled from the marginal distribution of scores for that particular question (covariate).

Table 3 describes the 16 primary factors. Each factor has 10 questions associated with it except trait B (Reasoning) which has 13 questions leading to a total of 163 questions.

Trait Name	Trait Code
Warmth	A
Reasoning	B
Emotional Stability	C
Dominance	E
Liveliness	F
Rule-Consciousness	G
Social Boldness	H
Sensitivity	I
Vigilance	L
Abstractedness	M
Privateness	N
Apprehension	O
Openness to change	Q1
Self-reliance	Q2
Perfectionism	Q3
Tension	Q4

Table 3: 16 PF Primary Factors

Here, we aim to model the network of 163 questions through a Potts model with 163 nodes. Each of the questions are evaluated on a scale of 1 to 5, resulting in a 5-colored Potts model. Our objective is to understand the associations between the questions by estimating the parameter matrix θ in the Potts model (1). We set the coupling function $C(z_r, z_j) = \frac{z_r z_j}{(4)^2}$ and marginal term $C(z_r) = \left(\frac{z_r}{4}\right)^2$, where $z_r \in (0, 1, \dots, 4)$ after shifting the origin to 0. The denominators in these terms help stabilize the computation of the log-likelihoods and the derivatives required in our MCMC computations. We run the MCMC sampler described in 3, with a burn-in of 10,000 iterations. The MCMC runs for 50,000 more iterations and we keep every 50th iteration to obtain a 1,000 MCMC samples.

The final strength of association between node (i, j) based on 1,000 samples is then mea-

sured through a single value $\tilde{\theta}_{ij}$ evaluated as in (9) which has values in the range of $(-20, 20)$. The heatmap of the strength of association ($\tilde{\theta}$) is given in Figure 7. The cluster of strong signals around the diagonal represents association between questions relating to the same personality trait while the sparse off-diagonal strong signals represent association between question that are related to two different personality traits. The percentage of non-zero estimates is around (6%).

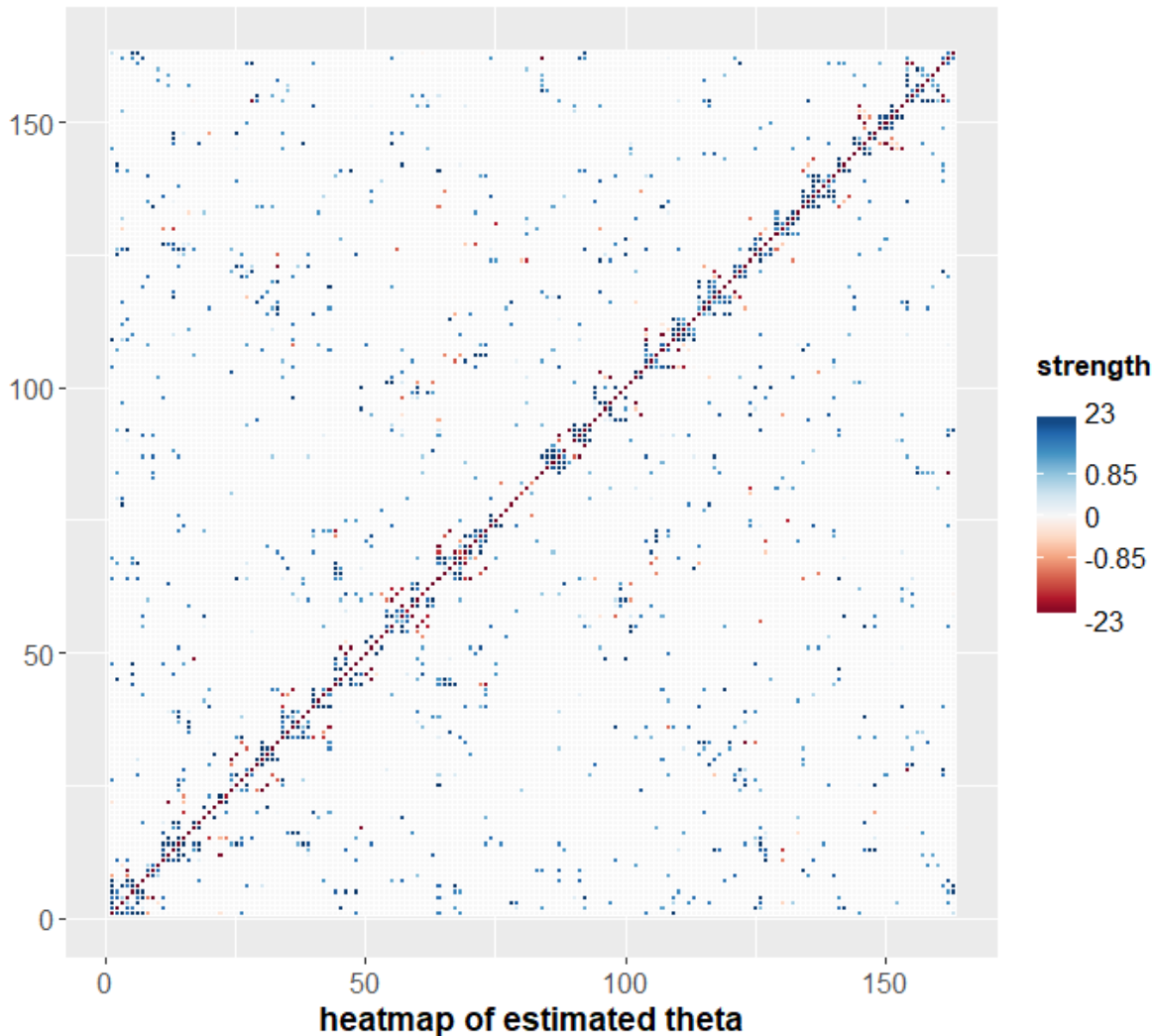


Figure 7: The heatmap of $\hat{\theta}$ after symmetrization (9)

The credible region for the estimate of θ_{ij} are evaluated as union of the 95% credible intervals of θ_{ij} and θ_{ji} , obtained from the MCMC samples of the respective posterior dis-

tributions. Figure 8 shows the estimated credible intervals for all the parameters (θ_{ij}) and Figure 9 is a zoomed in version of Figure 8 providing the estimated credible intervals for the parameters with $|\tilde{\theta}_{ij}| > 0.1$. It demonstrates the fact that for most inactive parameters the credible set is just a degenerate point at 0 thus providing high precision. Also the credible intervals tend to be symmetric around the estimates with higher absolute values (Figure 9).

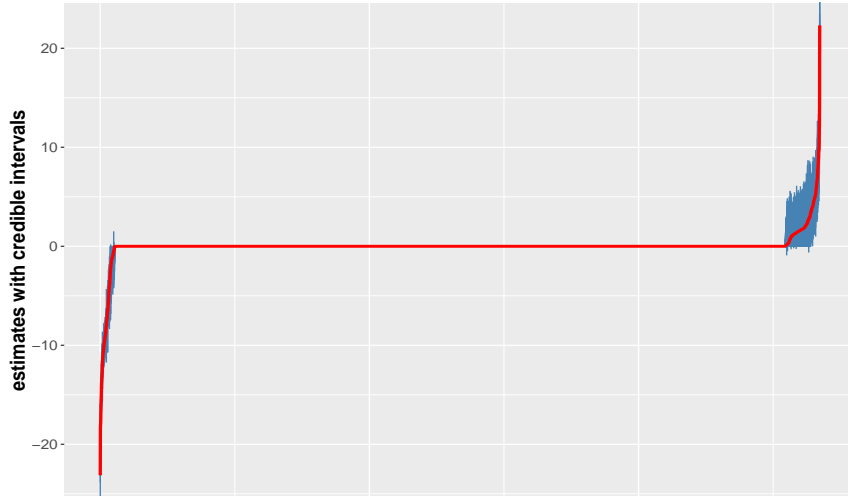


Figure 8: $\tilde{\theta}_{ij}$ (red) with credible intervals (blue) in order of strength of estimates

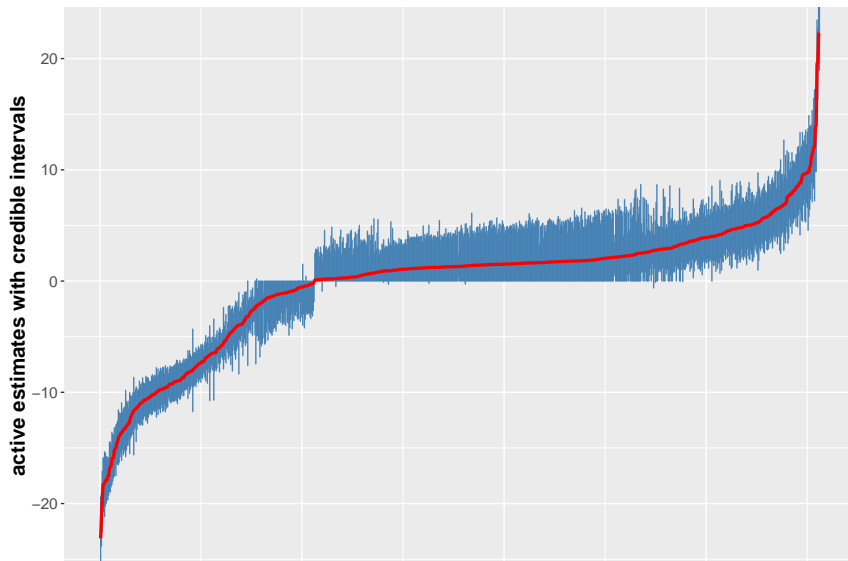


Figure 9: Figure 8 zoomed in for $|\tilde{\theta}_{ij}| > 0.1$

We estimate $\hat{P}(\delta_{ij} = 1)$ as proportion of the 1000 MCMC samples with $\delta_{ij} = 1$ and use Figure 10 to illustrate the credible intervals from the two posterior distributions for pairs of θ_{ij} and θ_{ji} for which probability of edge is calculated as in (11) is 1. For most cases, the two estimates are close with a high overlap between the credible intervals.

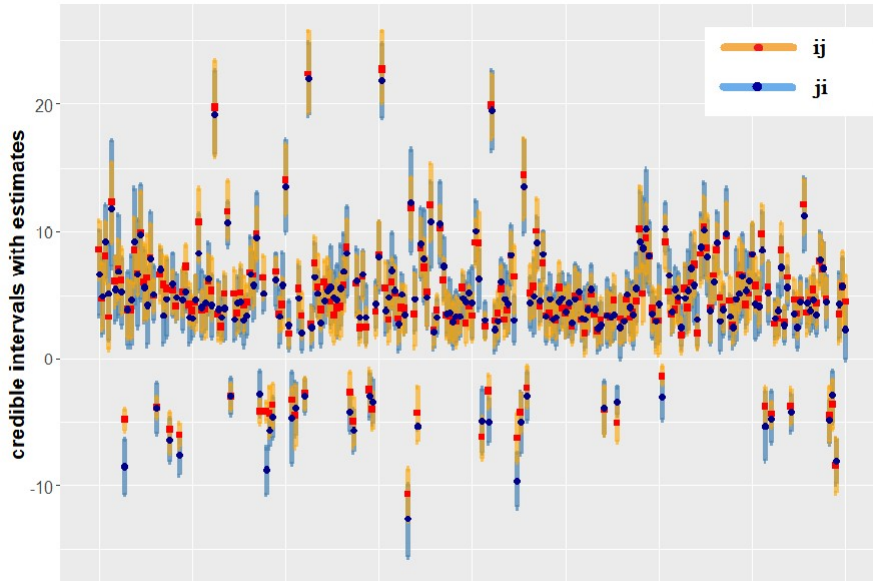


Figure 10: This plot shows $\hat{\theta}_{ij}$, $i \neq j$ for which probability of edge as calculated in (11) is 1. It presents $\hat{\theta}_{ij}$ (red) with credible interval (orange) and $\hat{\theta}_{ji}$ (blue) with credible interval (steelblue).

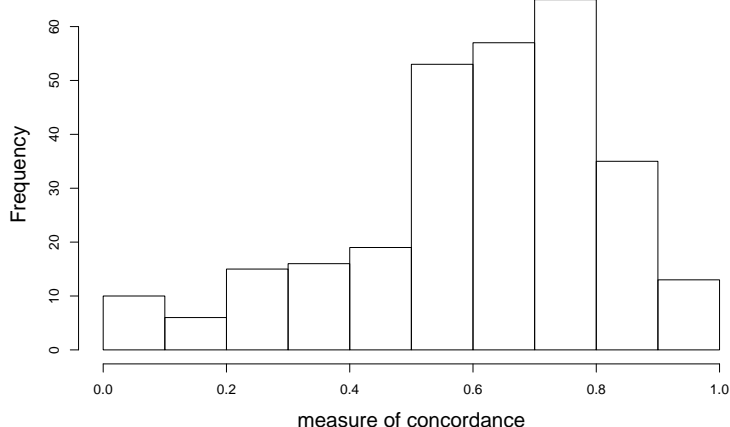


Figure 11: Empirical Distribution of measure of concordance between credible intervals for $|\hat{\theta}_{ij}| > .1$

The empirical distribution of the measure of concordance (10) is plotted in Figure 11. We observed that 84% of the estimated credible intervals had a high ($> 50\%$) measure of concordance. This indicates that the credible intervals of $\hat{\theta}_{ij}$ and $\hat{\theta}_{ji}$ are mostly in agreement with high overlap. Furthermore, the distribution also shows that only a small fraction (0.8%) of the estimates do not have intersecting credible intervals.

Cattell and Mead (2008) used several techniques including factor analysis to establish that personality structure is hierarchical, with primary and secondary level traits. The primary level consists of the 16 personality traits (used in our analysis). The secondary level consists of a version of the Big Five Traits corresponding to broader human qualities. They are obtained by factor-analyzing the correlation matrix of the 16 primary-level personality traits.

The grouping of the 16 primary factors into the Big Five Traits are shown in Table 4. Reasoning (trait B) stands alone without any association to the Big Five Traits.

Big Five Traits	Associated 16PF Traits
Introversion/Extroversion	A, F, H, N, Q2
Low anxiety/High Anxiety	C, L, O, Q4
Receptivity/Tough-Mindedness	A, I, M, Q1
Accommodation/Independence	E, H, L , Q1
Lack of Restraint/Self Control	F, G, M, Q3
–	B

Table 4: Grouping of the 16 primary factors into the Big Five Traits

With the results of the analysis we now wish to see if the 16 primary factors show similar associations as the ones established in Table 4. In order to do so, we start with our conservative estimate of the probability of edge between the questions (i, j) given by \hat{p}_{ij} (11). We summarize the estimates of probability of edge between 163 questions into a smaller 16×16 matrix ϕ corresponding to the 16 traits. We define the set $S_i = \{\text{questions under trait } i\}$ and n_{ij} to be the total number of possible edges between trait i and trait j . We define the matrix ϕ as

$$\phi_{ij} = \frac{1}{n_{ij}} \sum_{k \in S_i, l \in S_j} \hat{p}_{kl} \quad .$$

The off-diagonal elements of the matrix ϕ measure the average probability of association between each pair of traits. The element-wise reciprocal of this matrix gives us a pseudo-distance measure between the 16 traits which is used to form a hierarchical clustering using Ward’s method (`ward.D2` in `stats:hclust` in R). Figure 12 shows the results of the clustering. We see that our method perfectly recovers the introversion/extroversion (A, F, H, N, Q2) cluster. Additionally, (L, Q4) clustered together in our algorithm fall under anxiety in Table 4. Similarly, (I, Q1) clustered in our algorithm fall under receptivity/tough-mindedness in Table 4. Finally (G, M) cluster falls under Lack of Restraint/Self Control in Table 4. The cluster which is distinctly different (C, O, E, Q3, B) may lead to possible novel insights for the particular demographic that we chose for our study warranting further investigations. Thus we see a several groupings in 4 corresponding to the Big Five Traits are reflected in

our method.

The above clustering highlights that the δ_{ij} 's used in construction of the matrix ϕ , although auxiliary to the estimation of θ_{ij} 's, are well estimated through our MCMC sampler. This provides additional plausibility that the method outlined in this paper can estimate the underlying network with high precision.

6 Conclusion

In this article, we have used Potts model distribution to model networks with nodes taking discrete number of values. The use of pseudo-likelihood and independent prior on each parameter has enabled us to avoid the intractable normalization constant of the Potts model and perform computations in parallel for each node of the graph. In a high dimensional framework, the use of weak spike(Gaussian) and slab(Laplace) prior has helped in encoding sparsity in our estimated parameter matrix which is desirable for selection consistency. We have shown in our simulation settings that for specific choices of hyper-parameters, our MCMC algorithm recovers the true generating parameters and the method can achieve perfect F1 scores for moderate sample size. We have provided summary measures of estimates and credible intervals that resolve the issue of non-unique estimates of parameter θ_{ij} arising due to independent parallel computation on node i and j . Finally we have implemented the method on our 16 Personality Factor dataset and shown through a hierarchical clustering of our estimates that some of the important features of association between the 16 Personality Factors in captured in our estimates thus validating our inference. We have ongoing work on theoretical properties of quasi-posterior distribution under our choice of prior. In terms of MCMC algorithm, though our method works well in dimensions of $p = 300, n = 2,000$, it can be made faster if we choose a proposal distribution for inactive parameters that bypasses computation of the double derivative of the conditional likelihood, but we might loose sampling efficiency under such circumstances. We have ongoing work that improves the sampler in terms of computational efficiency.

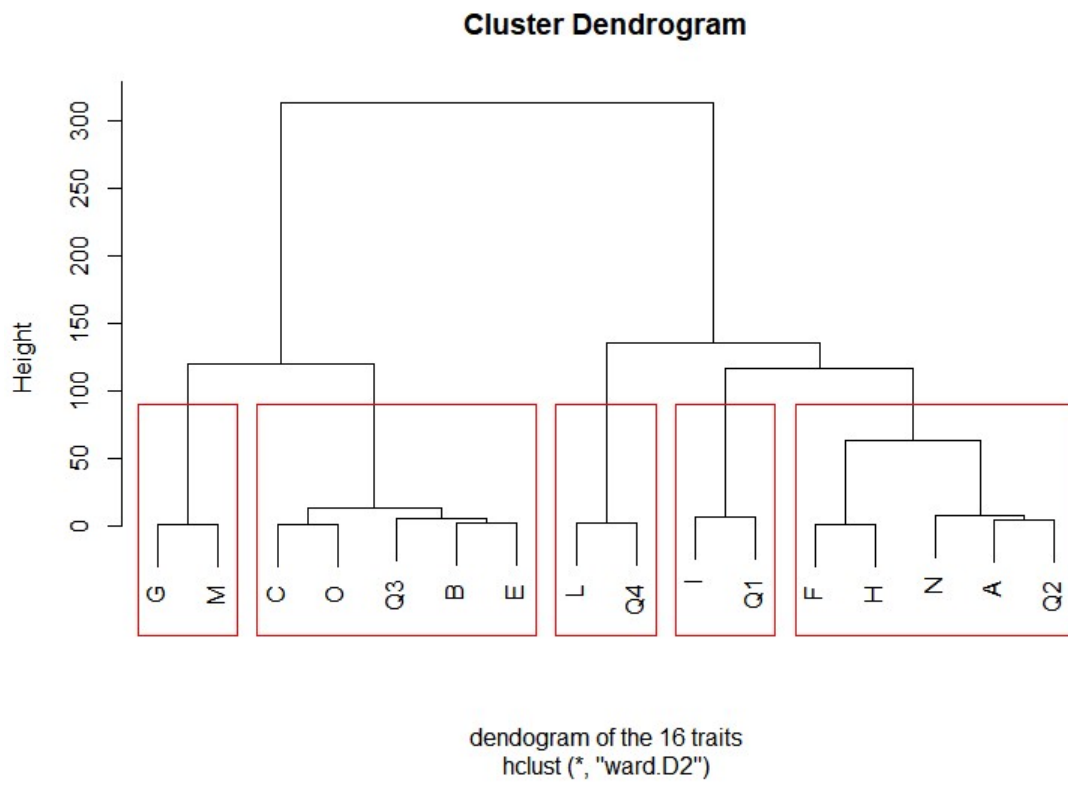


Figure 12: dendrogram identifying clusters of the 16 traits

7 Appendix

Appendix A: Computation of first and second derivatives for Potts Model

For an m colored Potts Model we re-write (2) as

$$f(z_r^i | z_{\setminus r}^i, \theta_r) = \exp(\langle \theta_r, C_r(z_r^i, z_{\setminus r}^i) \rangle - \Psi_r^i(\theta_r)) \quad (26)$$

where $C_r(z_r^i, z_{\setminus r}^i) \stackrel{\text{def}}{=} (C(z_r^i, z_1^i), \dots, C(z_r^i, z_{r-1}^i), C(z_r^i), C(z_r^i, z_{r+1}^i) \dots, C(z_r^i, z_p^i))$. $\Psi_r^i(\theta_r)$ denotes the normalization constant with respect to i_{th} observation and r_{th} node and is computed as

$$\Psi_r^i(\theta_r) = \sum_s \exp(\langle \theta_r, C_r(s, z_{\setminus r}^i) \rangle)$$

We define

$$\mathbf{E}_i[C_r(Z_r, z_{\setminus r}^i)] \stackrel{\text{def}}{=} \frac{\sum_s (C_r(s, z_{\setminus r}^i) \exp(\langle \theta_r, C_r(s, z_{\setminus r}^i) \rangle))}{\Psi_r^i(\theta_r)} = \nabla \log[\Psi_r^i(\theta_r)]$$

The negative log-likelihood for given data ($Z = z^{n \times p}$) can be computed as

Negative Log Conditional Likelihood

$$-\ell_r^n(\theta_r | z) = - \sum_{i=1}^n [\langle \theta_r, C_r(z_r^i, z_{\setminus r}^i) \rangle - \log \Psi_r^i(\theta_r)] \quad (27)$$

First derivative

$$-\nabla \ell_r^n(\theta_r | z) = - \sum_{i=1}^n \left[C_r(z_r^i, z_{\setminus r}^i) - \frac{\sum_{s=0}^{m-1} (C_r(s, z_{\setminus r}^i) \exp(\langle \theta_r, C_r(s, z_{\setminus r}^i) \rangle))}{\Psi_r^i(\theta_r)} \right] \quad (28)$$

$$= - \sum_{i=1}^n [C_r(z_r^i, z_{\setminus r}^i) - \mathbf{E}_i[C_r(Z_r, z_{\setminus r}^i)]] \quad (29)$$

Appendix B: Block update of the Non-Selected Parameters

The Matlab implementation (see Supplementary), shows that in our simulation settings, the acceptance probabilities at each node are quite high (85-90 %) and performing better than a multidimensional random walk. Using this block update scheme improves the runtime of the algorithm markedly. We also ensure that each block is not too large. The parameter **block** in our MATLAB implementation(see Supplementary) controls the size of the inactive blocks that are updated at a time. It is important to choose an optimal value for **block**, as having small **block** may decrease the computation time of each update but increases the total number of block updates required at each iteration, while a large **block** update is time-consuming but requires fewer updates. In our code,we usually select the parameter **block** to be around 10% of p .

SUPPLEMENTARY MATERIAL

Matlab-code: The matlab package with readme file is located at https://github.com/anwshaumich/DGM_parcomp/blob/master/software.zip

16PF data set: The Data set used for analysis in section 5 filtered to consider women between age between 30 to 50, self-reported accuracy of 75 or above and completion time less than half hour is called "smalldat.csv". After adjusting for the missing data we have the dataset "distmiss.csv". They are located at https://github.com/anwshaumich/DGM_parcomp/blob/master/16PF%20data%20used.zip

References

- Atchade, Y. (2015). A moreau-yosida approximation for high-dimensional posterior distributions. *Technical Report, University of Michigan*.
- Atchade, Y. (2017). On the contraction properties of some high-dimensional quasi-posterior distributions. *Annals of Statistics* 45, 2248–2273.

- Atchade, Y. F. (2006). An adaptive version for the metropolis adjusted langevin algorithm with a truncated drift. *Methodol. Comput. Appl. Probab.* 8, 235–254.
- Atchade, Y. F. and G. Fort (2012). Limit theorems for some adaptive mcmc algorithms with subgeometric kernels: Part ii. *Bernoulli* 18(3).
- Banerjee, O., L. El Ghaoui, and A. d’Aspremont (2008). Model selection through sparse maximum likelihood estimation for multivariate gaussian or binary data. *J. Mach. Learn. Res.* 9, 485–516.
- Besag, J. (1974). Spatial interaction and the statistical analysis of lattice systems. *J. Roy. Statist. Soc. Ser. B* 36, 192–236.
- Besag, J. (1986). On the statistical analysis of dirty pictures. *J. Roy. Statist. Soc. Ser. 48*, 259–302.
- Bottolo, L. and S. Richardson (2010). Evolutionary stochastic search for bayesian model exploration. *Bayesian Anal* 5, 583–618.
- Castillo, I., J. Schmidt-Hieber, and A. Van der Vaart (2015). Bayesian linear regression with sparse priors. *Annals of Statistics*. 43, 1986–2018.
- Cattell, H. and A. Mead (2008). Personality measurement and testing. *The SAGE Handbook of Personality Theory and Assessment* 2, 133–159.
- Chen, X., Z. J. Wang, and M. J. McKeown (2011). A bayesian lasso via reversible-jump MCMC. *Signal Processing* 91, 1920–1932.
- Ekeberg, M., C. Lövkvist, Y. Lan, and E. A. M. Weigt (2013). Improved contact prediction in proteins: Using pseudolikelihoods to infer potts models. *Physical Review* 87.
- George, E. I. and R. E. McCulloch (1997). Approaches to bayesian variable selection. *Statistica Sinica* 7, 339–373.
- Georgii, H.-O. (1988). Gibbs measures and phase transitions. *de Gruyter Studies in Mathematics* 9.

- Green, P. J. and S. Richardson (2002). Hidden Markov models and disease mapping. *J. Amer. Statist. Assoc.* *97*, 1055–1070.
- Greenfield, A., C. Hafemeister, and Bonneau, R. (2013). Robust data-driven incorporation of prior knowledge into the inference of dynamic regulatory networks. *Bioinformatics* *29*, 1060–1067.
- Guo, J., J. Cheng, E. Levina, G. Michailidis, and J. Zhu (2015, 06). Estimating heterogeneous graphical models for discrete data with an application to roll call voting. *Ann. Appl. Stat.* *9*(2), 821–848.
- Guyon, X. (1995). *Random fields on a network*. Probability and its Applications (New York). New York: Springer-Verlag. Modeling, statistics, and applications, Translated from the 1992 French original by Carenne Ludeña.
- Höfling, H. and R. Tibshirani (2009, 04). Estimation of sparse binary pairwise markov networks using pseudo-likelihoods. *Journal of machine learning research : JMLR* *10*, 883–906.
- Ising, E. (1925). Beitrag zur theorie des ferromagnetismus. *Zeitschrift Für Physik A Hadrons and Nuclei* *31*, 253–258.
- Kato, K. (2013). Quasi-bayesian analysis of nonparametric instrumental variables models. *Annals of Statistics* *41*, 2359–2390.
- Li, F. and N. R. Zhang (2010). Bayesian variable selection in structured high-dimensional covariate spaces with applications in genomics. *J. Amer. Statist. Assoc.* *105*, 1202–1214.
- Liu, J. (2001). Monte carlo strategies in scientific computing. *Springer*.
- Lyne, A., M. Girolami, Y. Atchade, H. Strathmann, and D. Simpson (2015). On russian roulette estimates for bayesian inference with doubly-intractable likelihoods. *Statistical Science* *30*, 443–467.
- Marin, J.-M., P. Pudlo, C. P. Robert, and R. J. Ryder (2012). Approximate bayesian computational methods. *Statistical Computing* *22*, 1167–1180.

- Meinshausen, N. and P. Bühlmann (2006). High-dimensional graphs with the lasso. *Annals of Stat.* *34*, 1436–1462.
- Mitchell, T. J. and J. J. Beauchamp (1988). Bayesian variable selection in linear regression. *J. Amer. Statist. Assoc.* *83*, 1023–1032.
- Murray, I., Z. Ghahramani, and D. MacKay (2006). MCMC for doubly-intractable distributions. *Proceedings of the 22nd Annual Conference on Uncertainty in Artificial Intelligence UAI06*, 359–366.
- Parikh, N. and S. Boyd (2013). Proximal algorithms. *Foundations and Trends in Optimization* *1*.
- Peng, B., D. Zhu, B. P. Ander, X. Zhang, F. Xue, F. Sharp, and X. Yang (2013). An integrative framework for bayesian variable selection with informative priors for identifying genes and pathways. *PLoS ONE* *8*(7).
- Ravikumar, P., M. J. Wainwright, and J. D. Lafferty (2010). High-dimensional Ising model selection using ℓ_1 -regularized logistic regression. *Ann. Statist.* *38*(3), 1287–1319.
- Robert, C. P. and G. Casella (2004). Monte carlo statistical methods. *Springer Texts in Statistics, Springer-Verlag, New York.*
- Roy, S., Y. Atchadé, and G. Michailidis (2017). Change point estimation in high dimensional markov random-field models. *Journal of the Royal Statistical Society: Series B (Statistical Methodology)* *79*(4), 1187–1206.
- Studham, M., A. Tjarnberg, T. Nordling, S. Nelander, and E. Sonnhammer (2014). Functional association networks as priors for gene regulatory network inference. *Bioinformatics* *30*, i130–i138.
- Zhou, X. and S. Schmidler (2009). Bayesian parameter estimation in ising and potts models: A comparative study with applications to protein modeling. *Technical Report*.